The Circadian Clock-Associated Small GTPase LIGHT INSENSITIVE PERIOD1 Suppresses Light-Controlled Endoreplication and Affects Tolerance to Salt Stress in Arabidopsis[1][W]

Kata Terecskei[2], Réka Tóth[2], Péter Gyula, Éva Kevei[3], János Bindics, George Coupland, Ferenc Nagy, and László Kozma-Bognár*

Institute of Plant Biology, Biological Research Centre of the Hungarian Academy of Sciences, H–6726 Szeged, Hungary (K.T., P.G., É.K., J.B., F.N., L.K.-B.); Department of Plant Developmental Biology, Max Planck Institute for Plant Breeding Research, D–50829 Cologne, Germany (R.T., G.C.); and School of Biological Sciences, University of Edinburgh, EH9 3JR Edinburgh, United Kingdom (F.N.)

Circadian clocks are biochemical timers regulating many physiological and molecular processes according to the day/night cycle. The small GTPase LIGHT INSENSITIVE PERIOD1 (LIP1) is a circadian clock-associated protein that regulates light input to the clock. In the absence of LIP1, the effect of light on free-running period length is much reduced. Here, we show that in addition to suppressing red and blue light-mediated photomorphogenesis, LIP1 is also required for light-controlled inhibition of endoreplication and tolerance to salt stress in Arabidopsis (*Arabidopsis thaliana*). We demonstrate that in the processes of endoreplication and photomorphogenesis, LIP1 acts downstream of the red and blue light photoreceptors phytochrome B and cryptochromes. Manipulation of the subcellular distribution of LIP1 revealed that the circadian function of LIP1 requires nuclear localization of the protein. Our data collectively suggest that LIP1 influences several signaling cascades and that its role in the entrainment of the circadian clock is independent from the other pleiotropic effects. Since these functions of LIP1 are important for the early stages of development or under conditions normally experienced by germinating seedlings, we suggest that LIP1 is a regulator of seedling establishment.

The optimal growth and development of plants are mediated by various signaling pathways that enable plants to modulate their molecular and physiological reactions in response to changes of the environment. Light, the sole energy source, is the most important environmental factor for plants. To monitor changes in ambient light conditions, plants evolved several families of photoreceptors covering the visible and the UV-A/B region of the spectrum (Franklin and Quail, 2010; Chaves et al., 2011; Rizzini et al., 2011). The red/far-red light-absorbing phytochromes (PhyA–PhyE) and the blue light-absorbing cryptochromes (CRY1 and CRY2) are considered to mediate the majority of physiological and developmental responses to visible light.

Besides regulating photomorphogenesis, these photoreceptors also play an essential role in entraining/synchronizing the circadian clock to the daily light/dark cycles (Devlin and Kay, 2000). This process is important, since the circadian clock is not a linear signaling system but rather modulates and coordinates signaling pathways and physiological processes through the day/night cycles (Covington et al., 2008). Synchronization of the clock with the objective time enables organisms to anticipate predictable changes of environmental parameters or the expected onset of stresses, which in turn may confer selective advantages (Dodd et al., 2005; Legnaioli et al., 2009).

The clock is a biochemical mechanism relying on the mutual feed-forward/feedback regulation of the so-called clock genes and proteins. The rhythm-generating module (also called the central oscillator) of the Arabidopsis (*Arabidopsis thaliana*) clock consists of at least three interconnected genetic circuits (Pruneda-Paz and Kay, 2010; Huang et al., 2012). In

addition to the basic transcriptional regulation, post-translational modifications, regulated proteolysis, or controlled nucleocytosolic transport of clock proteins also play important roles in the clock mechanism (Más, 2008; Wang et al., 2010). The central clockwork generates the primary oscillation in the expression of clock components with a period of about 24 h. The oscillation is then relayed to the expression of downstream components. In Arabidopsis, 15% to 25% of the transcriptome is regulated rhythmically. Circadian regulation is clearly overrepresented among the genes that are implicated in light, hormonal, or stress signaling, suggesting a molecular basis for the temporal modulation of these pathways (Covington et al., 2008).

Among these pathways, high-salinity stress represents ionic (high $[Na^+]$) and osmotic stress, and the responses of plant cells consist of several consecutive as well as parallel steps (Yamaguchi-Shinozaki and Shinozaki, 2006). The early responses involve an increase in Ca^{2+} flux leading to SALT OVERLY SENSITIVE (SOS) protein-mediated changes in ion homeostasis. Ca^{2+} flux and other secondary messengers such as phospholipids and reactive oxygen species (ROS) activate kinase signaling cascades triggering the transcription of rapid stress-inducible genes. These responses can be abscisic acid (ABA) dependent and independent, and both of these are linked to the circadian clock in several ways (Sanchez et al., 2011). For example, ABA induces *TOC1* expression at midday, which leads to circadian control of the ABA-related gene *ABA receptor/GENOMES UNCOUPLED5* (Legnaioli et al., 2009). This feedback mechanism ensures the correct timing and sensitivity of ABA signaling and stomata opening. As a consequence, TOC1 overexpression results in reduced ABA-mediated drought tolerance due to impaired stomata opening. Furthermore, ABA precursors, biosynthesis genes, and several ABA-responsive genes are diurnally expressed and show altered transcription in circadian clock mutants, like the *prr9,7,5* triple mutant or the CCA1 overexpressor (Fukushima et al., 2009). As for ABA-independent stress pathways, up-regulation of the *DEHYDRATION-RESPONSIVE ELEMENT B1/C-REPEAT-BINDING FACTOR* regulon was described in the *prr9,7,5* triple mutant, which displayed enhanced salt, drought, and cold tolerance (Nakamichi et al., 2009), whereas the same regulon was down-regulated in the *lhy cca1* double mutant, which exhibited reduced cold and salt tolerance (Kant et al., 2008; Dong et al., 2011). Hours after the onset of stress, a slower adaptation process starts, leading to stomata opening and the accumulation of osmolytes,
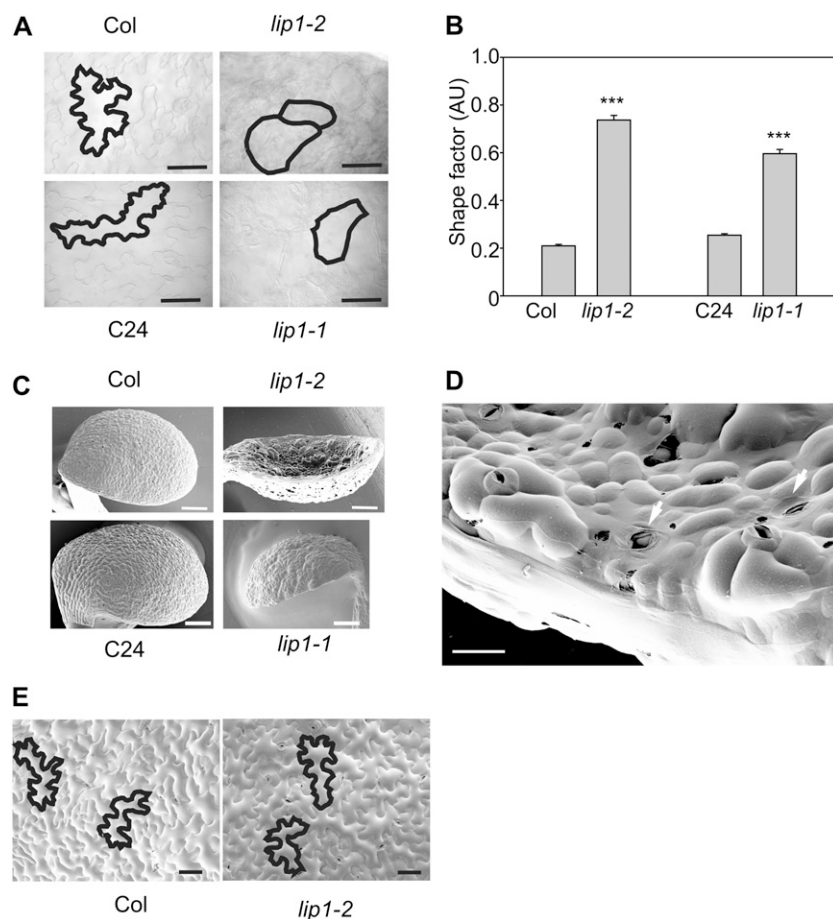
Figure 1. LIP1 regulates cell morphology in a developmental stage-specific manner. A, Pavement cell morphology in cotyledons of Col-0, *lip1-2*, C24, and *lip1-1* plants grown in 12:12 LD cycles for 7 d. Bars = 50 μm. B, Cell shape factor values calculated from the area and the perimeter of cotyledon pavement cells. n = 43 to 54; Student's t test $P < 0.001$ for both samples. Error bars represent SE. AU, Arbitrary units. C, Scanning electron microscopy images of cotyledons of Col-0, *lip1-2*, C24, and *lip1-1* plants grown in 12:12 LD cycles for 7 d. Bars = 200 μm. D, Scanning electron microscopy closeup image of a collapsed epidermal cell layer in the cotyledon of a *lip1-2* seedling grown in 12:12 LD cycles for 7 d. Arrows point at collapsed stomata guard cells. Bar = 20 μm. E, Scanning electron microscopy images of the first leaves of Col-0 and *lip1-2* plants grown in 12:12 LD cycles for 21 d. Bars = 50 μm.

secondary metabolites, and free radical scavengers, which protect the plant from stress damage.

Adaptation to the changing environment also requires plasticity of the developmental program both at the organism and cell levels. In fact, even core biochemical processes, such as the cell cycle, can be modulated by environmental factors. For example, in Arabidopsis, hypocotyl cells undergo several endocycles in the dark, but the last cycle is inhibited in the light (Gendreau et al., 1998). During this process, DNA replication is correctly initiated and terminated, but it is not followed by the separation of the chromosomes and cytokinesis (De Veylder et al., 2011). As a result, the cellular DNA is exactly doubled after each endocycle. Very recently, the light-regulated transcription of an atypical E2F transcription factor, DP-E2F-LIKE1 (DEL1), was proposed as the key mediator of light regulation of endoreplication (Berckmans et al., 2011). DEL1 transcription is positively or negatively regulated by the typical E2Fb or E2Fc transcription factor, respectively (Berckmans et al., 2011). E2Fb protein degradation is facilitated by the E3 ubiquitin ligase COP1, resulting in a low expression level of DEL1 in the dark. In the light, however, COP1 is inactivated by various photoreceptor-mediated mechanisms; thus, E2Fb protein levels rise, causing an increase in DEL1 transcription. DEL1 directly represses the transcription of FIZZY-RELATED1/CELL CYCLE SWITCH PROTEIN52 A2, which is an activator of the anaphase-promoting complex (APC; Lammens et al., 2008). APC is responsible for the degradation of mitotic cyclins leading to the inactivation of cyclin-cyclin-dependent kinase (CYC/CDK) complexes and the onset of endoreplication (De Veylder et al., 2011). Since DEL1 attenuates APC function mainly in the light, endoreplication is inhibited under these conditions.

Previously, we identified the small GTPase LIGHT INSENSITIVE PERIOD1 (LIP1) as a circadian clock-associated factor in Arabidopsis (Kevei et al., 2007). Loss of LIP1 function in the lip1-1 mutant severely reduced the effect of light on the shortening of free-running period length. Essentially, this resulted in a short-period phenotype of CHLOROPHYLL A/B-BINDING PROTEIN2:LUCIFERASE (CAB2:LUC) expression at low fluences of red and blue light. In this work, we provide physiological and molecular data demonstrating that (1) LIP1 is involved in mediating PhyB-controlled photomorphogenesis, (2) LIP1 is a component of the PhyB-controlled red light and CRY-controlled blue light signaling cascade inhibiting endoreplication, (3) LIP1 is required for the normal development of pavement cells in young seedlings, and (4) LIP1 function is needed for salt tolerance. Moreover, by manipulating the subcellular localization of LIP1, we show that the circadian function of LIP1 can be separated from its other functions not only at the physiological level but also at the cellular level.

RESULTS

Loss of Function of LIP1 Protein Causes Altered Cell Shape

Microscopic analysis of young lip1-1 and lip1-2 mutant seedlings (Kevei et al., 2007) revealed defects in cell development. In wild-type Arabidopsis plants, pavement cells have a characteristic jigsaw puzzle shape with lobes, whereas both in lip1-1 and lip1-2 mutants the cell shape is more rounded and much less complex (Fig. 1A). The shape factor, describing the roundness of the cells, indicated a significant difference between lip1 mutants and the corresponding wild types (Fig. 1B).
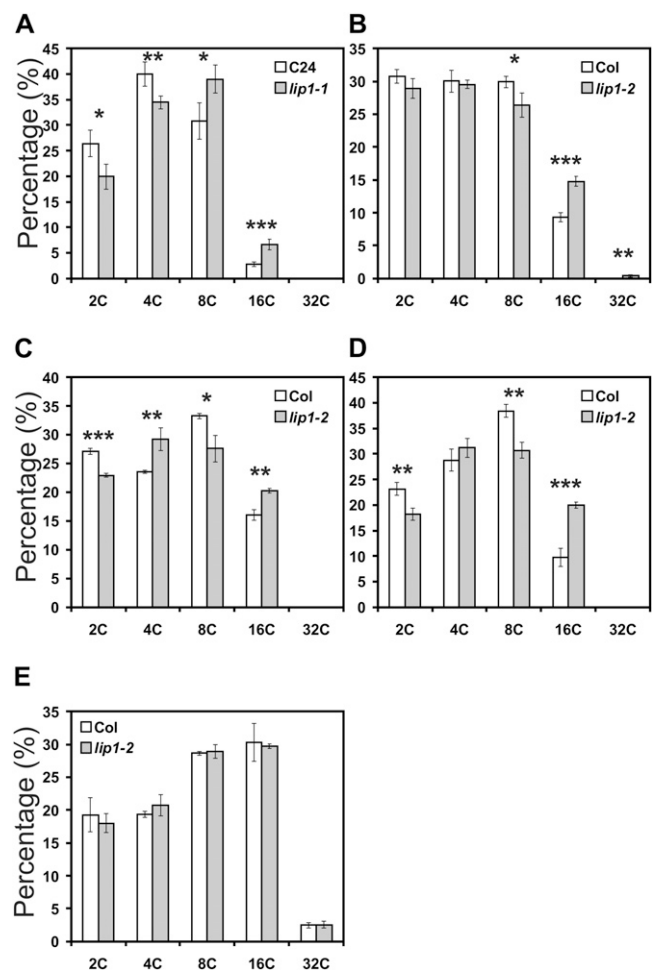
Figure 2. Increased ploidy levels in lip1 mutants. Ploidy levels were determined in different parts of 7-d-old wild-type and lip1 mutant seedlings: cotyledons (A and B), hypocotyls (C), or whole seedlings (D). Alternatively, ploidy levels were determined in the first leaves of 21-d-old Col-0 and lip1-2 plants (E). Plants were grown in 12:12 LD cycles. Relative ratios of nuclei with the indicated DNA content are plotted (n = 4). One sample contained 10 cotyledons (A and B), 10 hypocotyls (C), five seedlings (D), or four leaves (E). Asterisks indicate significant differences from the wild type as determined by Student's t test: *P < 0.05, **P < 0.01, ***P < 0.001. Error bars represent SD.

Additionally, we observed that *lip1-2* mutants showed characteristic, upward-curling cotyledons (Fig. 1C). This morphological change is the result of the noncontinuous layer of pavement and leaf blade cells that never occurs in wild-type plants (Fig. 1, C and D). This phenomenon is most likely caused by cell death, since the shapes of the stomata guard cells and pavement cells were still visible in the patches lacking epidermal cells (Fig. 1D). In fact, the remaining pavement cells form islands on the top of mesophyll cells (Supplemental Fig. S1). Unlike *lip1-2* seedlings (Fig. 1C), *lip1-1* plants displayed a continuous layer of pavement cells in the cotyledon, indicating ecotype-specific differences, as both mutant alleles are loss-of-function alleles (Kevei et al., 2007). In addition, our data suggest that the cell shape and discontinuous pavement cell layer phenotypes are developmentally regulated, because pavement cells in the first true leaves of *lip1-1* and *lip1-2* mutants had wild-type morphology (Fig. 1E). These observations suggest that LIP1 has a more pronounced function during the early developmental stages of the plant life cycle.

LIP1 Affects Ploidy Levels at the Seedling Stage

The alteration of cell morphology is frequently linked with changes in nuclear DNA content (Guimil and Dunand, 2007). Therefore, we analyzed ploidy patterns in the cotyledons of *lip1* mutants by flow cytometry and found that the proportion of nuclei having high DNA content was significantly increased in the mutants (Fig. 2, A and B). In particular, the ratio of 16C nuclei was elevated and, unlike in the wild type, even 32C nuclei were detectable in *lip1-2* cotyledons (Fig. 2B). Changes in ploidy levels are often associated with altered cell size or cell number. These parameters were determined for the pavement cells and the palisade mesophyll cells in *lip1-1* and wild-type cotyledons (Table I). Interestingly, elevated ploidy levels in *lip1-1* were accompanied by a reduction in the size of these cell types, but the total number of cells was not affected, suggesting that LIP1 does not affect the mitotic cell cycle. In agreement with the reduced cell size,

the area of *lip1-1* cotyledons was significantly smaller than that of the wild type (Table I). To test if nuclear DNA content is affected by LIP1 in other parts of the seedlings, samples of hypocotyls or entire seedlings were used in the assay (Fig. 2, C and D). Ploidy patterns in isolated hypocotyls of the *lip1-2* mutant showed the same tendency as in the cotyledons, demonstrating that in the seedling stage the effect of LIP1 on endoreplication is not organ specific. In contrast, ploidy patterns in the matured first leaves of *lip1-2* and wild-type plants were not significantly different (Fig. 2E), suggesting that LIP1 suppresses ploidy levels in a developmentally regulated manner.

## Light-Dependent Inhibition of Endoreplication by LIP1

Four cycles of endoreplication could occur in dark-grown Arabidopsis seedlings, whereas the fourth cycle is inhibited in light (Gendreau et al., 1998). Since LIP1 is involved in the light regulation of the circadian clock and photomorphogenic processes (Kevei et al., 2007), we analyzed ploidy patterns in *lip1* mutants grown under different light conditions. Elevated ploidy level was detected in *lip1* seedlings grown under light/dark cycles (Fig. 3, C and D), and the DNA content increased further when plants were grown in continuous white light (Fig. 3, E and F). However, ploidy levels were identical in etiolated *lip1* and wild-type seedlings (Fig. 3, A and B), demonstrating that LIP1 suppresses endoreplication in a light-dependent manner. We also characterized pavement and palisade mesophyll cells in the cotyledons of etiolated C24 and *lip1-1* seedlings. In contrast to light-grown plants (Fig. 1A; Table I), the shape, number, and size of these cells types were not significantly different in the wild-type and mutant seedlings grown in the dark (Table II; Supplemental Fig. S2). These results demonstrate that the cell morphology phenotype of *lip1* mutants is light dependent.

In red light, the light-induced inhibition of endoreplication depends on the photoreceptor PhyB, as dark- or red light-grown *phyB* mutants have identical, high ploidy levels (Gendreau et al., 1998). To test the epistatic relation between LIP1 and PhyB in controlling

Table I. *Quantitative characterization of pavement and palisade mesophyll cells on the adaxial surface of cotyledons of light-grown seedlings*

Wild-type and *lip1-1* seedlings were grown in 12:12 LD cycles for 7 d. Digital images were taken of the whole cotyledon or different areas and focal planes of the adaxial surface. The size of cotyledons ($n = 12–15$) and cells at similar positions in the cotyledon ($n = 16–22$ per cotyledon) were measured. The number of pavement and palisade cells was calculated by dividing the total cotyledon area by the average area of the particular cell type. Mean values ± SD are shown. The significance of the differences from the wild type was analyzed by Student's *t* test, and corresponding *P* values are shown.

Genotype	Cotyledon Size	Pavement Cells		Palisade Cells	
		No.	Size	No.	Size
	mm^2		μm^2		μm^2
C24 (wild type)	2.082 ± 0.176	561 ± 61	3,697 ± 202	1,797 ± 253	1,165 ± 156
lip1-1	1.568 ± 0.194	528 ± 77	2,874 ± 175	1,894 ± 310	821 ± 129
P	<0.001	0.53	<0.001	0.29	0.0041
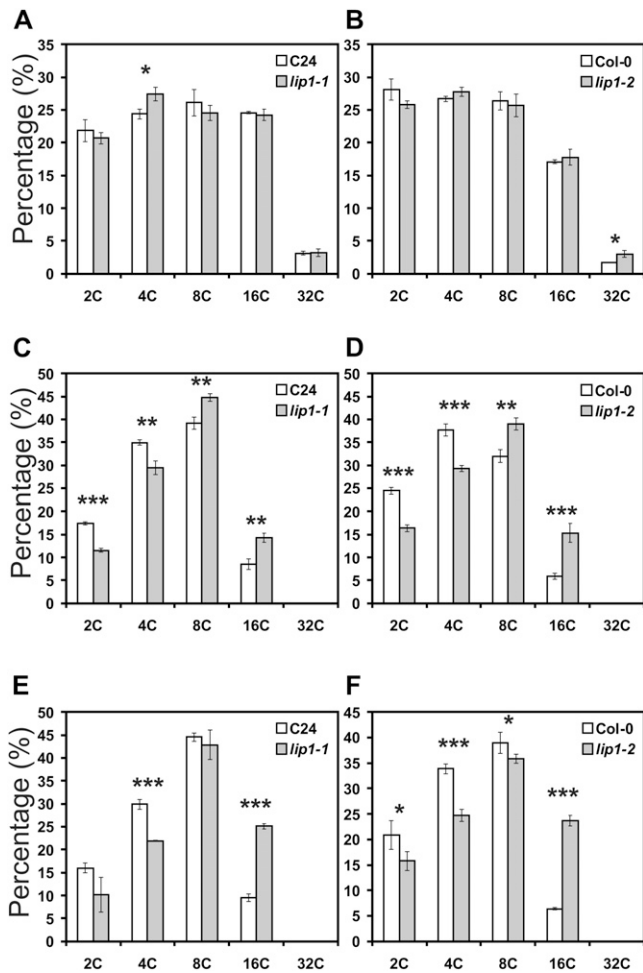
Figure 3. The effect of LIP1 on ploidy levels is light dependent. C24 and *lip1-1* (A, C, and E) or Col-0 and *lip1-2* (B, D, and F) plants were grown in darkness (A and B), in 12:12 LD cycles (C and D), or in continuous white light (E and F) for 6 d. Whole seedlings were used for ploidy level determinations. Data were obtained and analyzed as for Figure 2 (*n* = 4). Asterisks indicate significant differences from the wild type as determined by Student's *t* test: *P < 0.05, **P < 0.01, ***P < 0.001. Error bars represent SD.

red light-dependent endoreplication, ploidy levels of *lip1-2* and *phyB-9* single mutants and *lip1-2 phyB-9* double mutants were compared. In continuous red light (cR), both *lip1-2* and *phyB-9* mutants showed similarly increased ratios of 16C and 32C nuclei (Fig. 4B). Importantly, the *lip1-2 phyB-9* double mutant did not display an additive phenotype but phenocopied the *phyB-9* single mutant in cR (Supplemental Fig. S3). The DNA content of these mutants grown in darkness displayed patterns like wild-type seedlings, confirming the light-specific effect of the mutations (Fig. 4A).

Next, we examined whether LIP1 affects endoreplication in other light conditions, such as in continuous blue light (cB) or continuous far-red light (cFR). Ploidy levels of *lip1-2* mutant showed significant increases in cB (Fig. 4D; Supplemental Fig. S4), but it was

indistinguishable from the wild type in cFR (Fig. 4E). To place LIP1 in the light signaling pathway, the mutation in the *LIP1* gene was combined with the mutations in genes coding for the blue light-absorbing CRY1 and CRY2 or far-red light-sensing PhyA receptors, and seedlings were tested in cB or cFR. In cB, the ploidy pattern of the *lip1-2 cry1 cry2* triple mutant was most similar to that of the *cry1 cry2* double mutant (Fig. 4D; Supplemental Fig. S4), suggesting that LIP1 is epistatic to the CRY photoreceptors. In cFR, the *lip1-2 phyA-211* double mutant phenocopied the *phyA-211* single mutant (Fig. 4E), further supporting the previous finding that LIP1 is not involved in far-red light-specific control of endoreplication. In summary, these results indicate that LIP1 plays an important role in integrating red and blue light signals to inhibit endoreplication. Furthermore, LIP1 is likely to function downstream of PhyB and CRY photoreceptors.

The light-regulated transcription of the atypical E2F transcription factor DEL1 was suggested to play a key role in the light regulation of endoreplication (Berckmans et al., 2011). To test the involvement of LIP1 and PhyB in light-regulated transcription of DEL1, we determined levels of *DEL1* mRNA in the wild type and in *lip1-2*, *phyB-9*, and *lip1-2 phyB-9* mutants grown in darkness or cR. In wild-type plants, *DEL1* mRNA levels were higher in the light than in darkness (Fig. 4F), in agreement with previous results (Berckmans et al., 2011). Interestingly, the red light-induced up-regulation of *DEL1* expression was clearly detectable in all genotypes, including the *phyB-9* single mutant. Furthermore, *DEL1* mRNA levels in any of the tested mutants showed no significant differences compared with the wild type (Fig. 4F). These data suggest that in red light, LIP1 and PhyB do not inhibit endoreplication through the transcriptional control of *DEL1*.

The Function of LIP1 in Controlling Photomorphogenesis Depends on PhyB, CRY1, and CRY2 But Is Independent of PhyA

It had been demonstrated that *lip1-1* mutants show elevated photomorphogenic responses (short hypocotyls) to red and blue light but not to far-red light (Kevei et al., 2007). In order to place the action of LIP1 in light signaling pathways mediated by phytochrome and cryptochrome photoreceptors, we characterized the responsiveness of *lip1-2 phyB-9*, *lip1-2 phyA-211*, and *lip1-2 cry1 cry2* multiple mutants to red, far-red, and blue light, respectively. In cR, the *lip1-2* mutant showed significantly shorter hypocotyls than the wild type; however, the *lip1-2 phyB-9* double mutant produced hypocotyls much longer than the wild type and was very similar to that of the *phyB-9* single mutant (Fig. 5A; Supplemental Fig. S5A). In cB, the *lip1-2* mutant displayed less pronounced but significant hypersensitivity compared with the wild-type, but *lip1-2 cry1 cry2* produced long hypocotyls similar to the *cry1 cry2* double mutant (Fig. 5B; Supplemental Fig. S5B).

Table II. *Quantitative characterization of pavement and palisade mesophyll cells on the adaxial surface of cotyledons of etiolated seedlings*

Wild-type and *lip1-1* seedlings were grown in darkness for 7 d. Digital images were taken of the whole cotyledon or different areas and focal planes of the adaxial surface. The size of cotyledons (n = 9–11) and cells at similar positions in the cotyledon (n = 35–60 per cotyledon) were measured. The number of pavement and palisade cells was calculated by dividing the total cotyledon area by the average area of the particular cell type. Mean values $\pm$ SD are shown. The significance of the differences from the wild type was analyzed by Student's t test, and corresponding P values are shown.

Genotype	Cotyledon Size	Pavement Cells		Palisade Cells	
		No.	Size	No.	Size
	mm^2		μm^2		μm^2
C24 (wild type)	0.229 ± 0.039	581 ± 75	394 ± 61	1,423 ± 281	161 ± 31
lip1-1	0.207 ± 0.031	549 ± 83	368 ± 69	1,321 ± 235	136 ± 27
P	0.09	0.47	0.39	0.18	0.12

In cFR, *lip1-2* phenocopied wild-type plants, and the *lip1-2 phyA-211* double mutant showed hypocotyl lengths identical to those of the *phyA-211* mutant (Fig. 5C; Supplemental Fig. S5C). These data verify that LIP1 does not affect PhyA-dependent far-red light signaling. The photomorphogenic phenotype of *lip1* mutants in red light is mainly due to the perturbation of PhyB-mediated signaling, whereas the *lip1* phenotype in blue light depends on the CRY photoreceptors. Absolute hypocotyl length data are provided in Supplemental Figure S6.

lip1 Mutants Are Hypersensitive to Salt Stress

In order to obtain additional information on the function of LIP1, we determined the responsiveness of *lip1* mutants to different abiotic stress conditions. We found that *lip1* mutants grown under 12-h-light/12-h-dark (12:12 LD) cycles displayed an increased sensitivity to salt (NaCl) stress (Fig. 5, D and E; Supplemental Fig. S7). Wild-type plants could tolerate 100 mM NaCl, but the growth and development of mutant *lip1* seedlings were greatly impaired under these conditions (Supplemental Fig. S7). *lip1-1* mutants were slightly less sensitive to NaCl than *lip1-2* mutants, which is probably due to ecotype-specific differences, as wild-type C24 seedlings appeared to be more tolerant than ecotype Columbia-0 (Col-0; Supplemental Fig. S7). In addition to poor growth and development, the germination rate of *lip1-2* seedlings was also significantly reduced under salt stress conditions as compared with the wild type (Fig. 5E). To test if light conditions modulate this stress response, germination rate was also analyzed in dark-grown plants. Under these conditions, *lip1-2* mutants were again more sensitive than wild-type plants (Fig. 5E), indicating that the salt stress phenotype is not caused by other light-dependent defects of *lip1* mutants (e.g. ploidy levels). Besides inhibiting germination, high NaCl concentration also attenuates root growth; therefore, we determined this response of *lip1* mutants grown on different concentrations of NaCl. Figure 5F illustrates that the relative inhibition of root growth is significantly stronger in the *lip1* mutants than in the wild type. These data demonstrate that LIP1 is required for maximum tolerance to salt stress.

High salinity represents osmotic and ionic stress for plants. Osmotic stress leads to the induction of osmoprotectant genes like *RESPONSIVE TO DESICCATION29A (RD29A)*, *RD29B*, or *RESPONSIVE TO ABA18 (RAB18)*, whereas ionic stress (increase in the cellular [Na^+]) induces the transcription of *SOS2*, an activator of the Na^+/H^+ transporter SOS1. To test if LIP1 participates in any of these processes, 1-week-old wild-type and *lip1-2* plants were transferred to medium containing 200 mM NaCl. Salt-induced expression of *RD29A*, *RD29B*, *RAB18*, and *SOS2* genes was monitored by quantitative reverse transcription (qRT)-PCR. Supplemental Figure S8 demonstrates that there were no significant differences in the kinetics or the level of induction of these genes. These results indicate that LIP1 plays a minor role, if any, in sensing salt stress signals and the transcriptional activation of the salt stress-related genes tested. However, an effect of LIP1 on the posttranslational modification, turnover, or subcellular localization of these components cannot be excluded.

Subcellular Localization of LIP1

We showed previously that the yellow fluorescent protein (YFP)-LIP1 fusion protein is detectable both in the cytosol and in the nucleus and that this distribution pattern is not significantly affected by light conditions or the circadian clock (Kevei et al., 2007). In order to test if any of the pleiotropic functions of LIP1 described above require specific subcellular localization, we generated transgenic *lip1* plants expressing the LIP1-YFP fusion protein with or without a nuclear localization signal (NLS) or a nuclear export signal (NES; Supplemental Fig. S9A) Transgenic lines with comparable expression levels were selected (Supplemental Fig. S9B), and localization of the different LIP1 fusion proteins was analyzed by fluorescence microscopy. As expected, YFP-LIP1 was detectable both in the cytoplasm and in the nuclei, whereas YFP-LIP1-NLS and YFP-LIP1-NES were
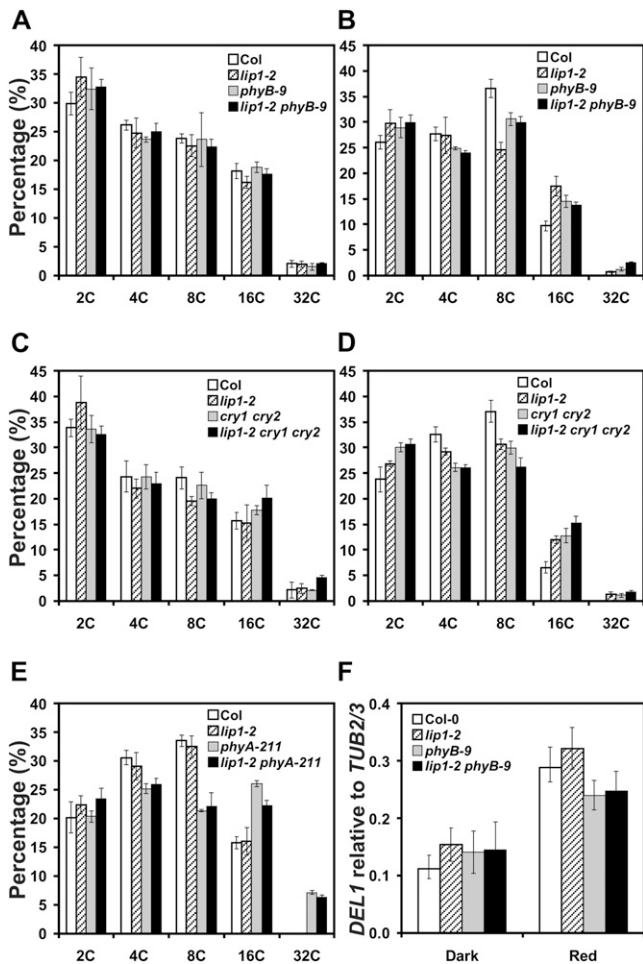
Figure 4. LIP1 attenuates endoreplication in red and blue light but not in far-red light. A to E, Plants of the indicated genotypes were grown in darkness (A and C), in cR (40 μmol m^{-2} s^{-1}; B), in cB (40 μmol m^{-2} s^{-1}; D), or in cFR (5 μmol m^{-2} s^{-1}; E) for 7 d. Whole seedlings were subjected to ploidy level determinations. Data were obtained and analyzed as for Figure 2 (n = 3–5). Results of statistical analysis (one-way ANOVA, Tukey's test) are shown in Supplemental Figures S3 and S4. Error bars represent SD. Ploidy levels in dark-grown *phyA-211* or *lip1-2 phyA-211* plants were not different from those in Col-0 or *lip1-2* plants (data not shown). F, Plants were grown in conditions identical to those for A and B. Expression levels of *DEL1* were determined by qRT-PCR assays. Values were normalized to *TUB2/3* mRNA levels. Averages of three independent experiments are shown. Error bars represent SE. Results of Student's *t* tests indicated that differences between the wild type and any mutant combinations under a given light condition (dark or red light) were not significant ($P > 0.1$ for any combination).

clearly restricted to the nucleus and the cytoplasm, respectively (Supplemental Fig. S9C).

Nuclear Localization of LIP1 Is Essential for the Circadian Function of the Protein

Complementation of the ploidy, salt stress, photomorphogenic, and circadian phenotypes of the *lip1*

mutants was tested in the selected transgenic lines. Figure 6A demonstrates that the expression of YFP-LIP1, YFP-LIP1-NLS, or YFP-LIP1-NES in the *lip1* mutant background restored ploidy levels to the wild-type level, best illustrated by the ratio of nuclei having 16C or 32C DNA content. In addition to ploidy levels, the characteristic jigsaw shape of cotyledon pavement cells was also restored in all complemented lines (Supplemental Fig. S10). Furthermore, *lip1-2* plants expressing either of the LIP1 fusion proteins were able to tolerate 100 mM NaCl and develop similarly to wild-type plants (Fig. 6B). Hypocotyl lengths of either of the complemented lines grown in red, blue, or far-red light were also indistinguishable from that of the wild type (Fig. 7, A–C). These data suggest that compartmentalization of LIP1 is not sufficient to abrogate LIP1 function for mediating these responses. However, the compartmentalization of LIP1 distinguishes its function concerning circadian rhythmicity (Fig. 7, D–F; Table III). The expression of YFP-LIP1 or YFP-LIP1-NLS restored wild-type circadian rhythms, whereas YFP-LIP1-NES-expressing transgenic *lip1-2* seedlings displayed rhythms very similar to that of *lip1-2*. Period estimates quantitatively demonstrated full complementation or the complete lack of complementation as indicated (Table III). We conclude that for the regulation of the circadian clock, a significant portion of LIP1 needs to be present in the nucleus. These observations suggest that the function of LIP1 in the circadian clock can be separated from its role in the control of cell development, endoreplication, stress tolerance, and photomorphogenesis.

DISCUSSION

The *lip1-1* mutant was identified in a genetic screen designed to isolate novel circadian clock mutants in Arabidopsis (Kevei et al., 2006, 2007). The *lip1-1* mutation shortened the free-running period of *CAB2:LUC* in low-intensity red light, and the mutant showed hypersensitive photomorphogenic responses in red and blue light. In this paper, we demonstrate that the *lip1-1* and *lip1-2* mutants display additional pleiotropic phenotypes and that LIP1 also plays important roles in the light-controlled inhibition of endoreplication and providing tolerance to salt stress.

It has been shown that far-red and red light perceived by the PhyA and PhyB photoreceptors inhibit the last round of endocycles in hypocotyl cells in Arabidopsis, whereas the receptor mediating the effect of blue light was not identified unequivocally (Gendreau et al., 1998). *lip1* mutants showed higher ploidy levels in white, red, and blue light but not in darkness or in far-red light (Figs. 3 and 4). This indicates that the ploidy phenotype of *lip1* mutants arose from the impaired red and blue light control of endoreplication. In fact, genetic analysis of red and blue light-controlled ploidy patterns demonstrated that *PHYB*, *CRY1*, and *CRY2* are epistatic to *LIP1* (Fig. 4). This suggests that
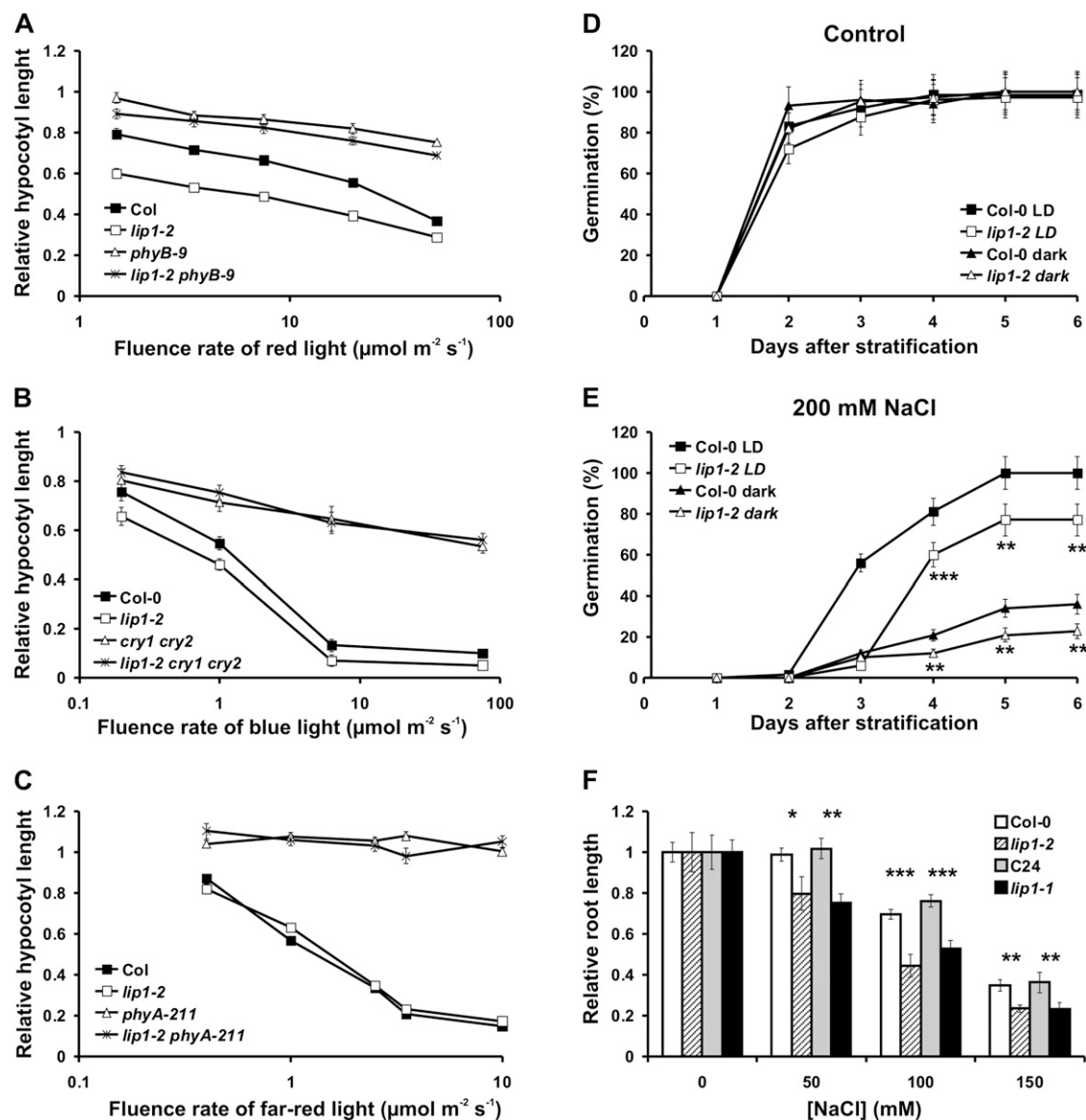
Figure 5. Physiological responses to light and salt stress are altered in *lip1* mutants. A to C, Plants were grown in cR (A), cB (B), or cFR (C) at the indicated fluence rates for 4 d, then hypocotyl length of the seedlings was measured. Values were normalized to the hypocotyl length of the corresponding dark-grown seedlings. The *x* axes show logarithmic scale. Error bars represent SE (*n* = 28–32). Results of statistical tests (one-way ANOVA, Tukey's test) for A to C are shown in Supplemental Figure S5. D and E, Col-0 and *lip1-2* mutant seeds were grown in 12:12 LD cycles or continuous darkness (dark) on medium with or without 200 mM NaCl. The number of seedlings with emerged radicles was counted daily and expressed as the percentage of the total number of seeds. Error bars represent SE (*n* = 105–125). F, Col-0, *lip1-2*, C24, and *lip1-1* seedlings were grown in 12:12 LD cycles for 7 d and transferred to vertical plates with medium supplemented with different concentrations of NaCl, as indicated. Root lengths were measured 7 d after the transfer. Values normalized to the root length of plants grown on salt-free medium are shown. Error bars represent SE (*n* = 17–20). For D to F, asterisks indicate significant differences from the wild type as determined by Student's *t* test: *P < 0.05, **P < 0.01, ***P < 0.001.

LIP1 functions as a component of the PhyB-, CRY1-, and CRY2-mediated light signaling pathways leading to the inhibition of endoreplication. Apart from the receptors, the atypical E2F transcription factor DEL1 was recently shown to mediate light-dependent endoreplication (Berckmans et al., 2011). In particular, the transcription of *DEL1* is light induced and

negatively correlated with ploidy levels, and ectopically expressed *DEL1* uncouples the regulation of endoreplication from light signals (Berckmans et al., 2011). Here, we show that the level of *DEL1* mRNA in *phyB-9*, *lip1-2*, and *lip1-2 phyB-9* plants was not significantly different from that in wild-type plants (Fig. 3). These data demonstrate that red light-induced
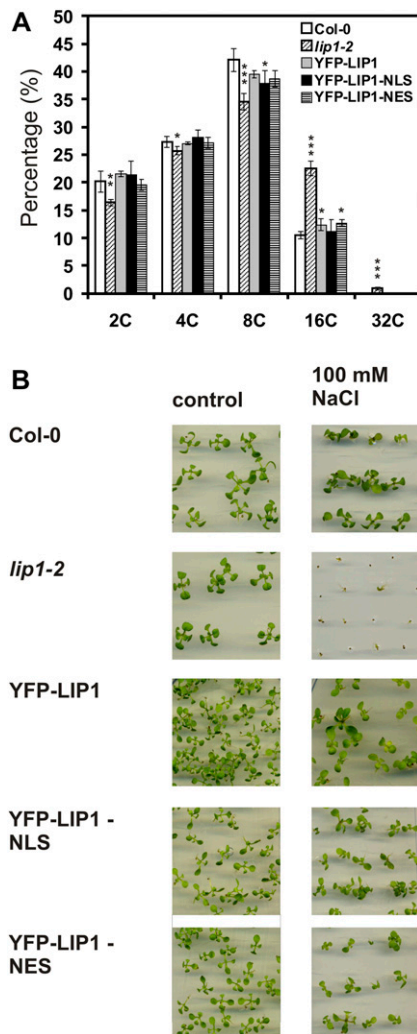
Figure 6. Complementation of ploidy and salt stress phenotypes of *lip1-2* by LIP1 fusion proteins. A, Ploidy levels in Col-0, *lip1-2* mutant, and *lip1-2* mutant expressing YFP-LIP1, YFP-LIP1-NLS, or YFP-LIP1-NES fusion proteins. Plants were grown in continuous white light (80 μmol m^{-2} s^{-1}) for 7 d ($n = 4$). Asterisks indicate significant differences from the wild type as determined by Student's t test: *$P < 0.05$, **$P < 0.01$, ***$P < 0.001$. Error bars represent SD. B, Seedlings expressing YFP-LIP1, YFP-LIP1-NLS, or YFP-LIP1-NES fusion proteins in the *lip1-2* mutant background along with Col-0 and *lip1-2* controls were grown in 12:12 LD cycles for 14 d on medium with or without 100 mM NaCl.

inhibition of endoreplication by PhyB and LIP1 define a pathway independent of the transcriptional regulation of *DEL1*.

Changes in ploidy levels are often accompanied by altered shape or size of the cells. In fact, we showed that pavement cells in the cotyledons of *lip1* mutants are significantly smaller and more rounded (or less lobed) compared with those in wild-type plants. The cell morphology phenotype of *lip1* mutants appears to closely correlate with ploidy changes, since both phenotypes are developmentally regulated and light dependent in the same manner. In wild-type plants, cells

with higher ploidy levels are usually larger, but there are several examples from mutants where increased ploidy levels are not accompanied by growth promotion or the size of particular cells is enlarged without significant increase of DNA content (De Veylder et al., 2011). Moreover, strong overexpression of Kip-Related Protein2 (KRP2), an inhibitor of CDKA;1, resulted in lower ploidy levels but larger pavement cells (Verkest et al., 2005). *lip1* mutants represent a novel class of exceptions, where cells with higher ploidy levels are apparently smaller in size. These observations collectively suggest that cellular DNA content does not control cell expansion directly but probably sets the range or capacity of future cell growth, which is influenced by the coaction of several additional factors.

In order to shed light on the molecular background of the salt sensitivity of *lip1* mutants, the function of the canonical osmotic and ionic stress signaling pathway was probed. As, in the *lip1* mutants, salt stress induced the transcription of both ABA-dependent and independent stress-related genes normally (Supplemental Fig. S8), we suggest that stress perception, signaling cascade, and transcriptional activation of the multiple pathways were not impaired by the lack of LIP1 function. Rather, LIP1 could affect one of the late stress-induced processes at the cellular level. A likely target of LIP1 action could be the regulation of ROS production, as small GTPases are involved in this process in animals, yeast, and plants as well (Finkel, 2006). A RHO OF PLANTS (ROP)-type small GTPase, RAC-LIKE1 (OsRAC1) in rice (*Oryza sativa*), was shown to directly interact with NADPH oxidase and hence modulate ROS production (Wong et al., 2007). OsRAC1 and its Arabidopsis homolog ROP2 exhibit altered responses to biotic and abiotic stresses accompanied by apoptosis-like cell death (Ono et al., 2001; Park et al., 2004). In addition to stress sensitivity, the *lip1-2* mutant also shows cell death symptoms, although this is restricted to the cotyledon epidermis cells (Fig. 1; Supplemental Fig. S1), unlike the necrotic lesions on leaves observed in dominant negative RAC1. Furthermore, the

Table III. *Period estimates for CAB2:LUC reporters in wild-type, lip1-2, and different YFP-LIP1 fusion protein-expressing plants*

Seedlings were grown under 12:12 LD cycles for 7 d and moved to cR (3 μmol m^{-2} s^{-1}). Period estimates were calculated by the Biological Rhythms Analysis Software System, developed in Andrew Millar's group, and it can be downloaded from http://millar.bio.ed.ac.uk. Three independent transgenic lines were analyzed for each complementing construct. A total of 32 individual seedlings were measured for each line. Variance-weighted mean periods and SE are shown. The significance of the differences from the wild type ($P^{[Col-0]}$) or the *lip1-2* mutant ($P^{[lip1-2]}$) was analyzed by Student's t test.

Genotype	Period	$P^{[Col-0]}$	$P^{[lip1-2]}$
	h		
Col-0 (wild type)	29.95 ± 0.28	–	<0.001
lip1-2	27.37 ± 0.77	<0.001	–
YFP-LIP1 [*lip1-2*]	29.74 ± 0.36	0.76	0.0023
YFP-LIP1-NLS [*lip1-2*]	29.33 ± 0.70	0.22	0.0061
YFP-LIP1-NES [*lip1-2*]	27.42 ± 0.31	<0.001	0.71
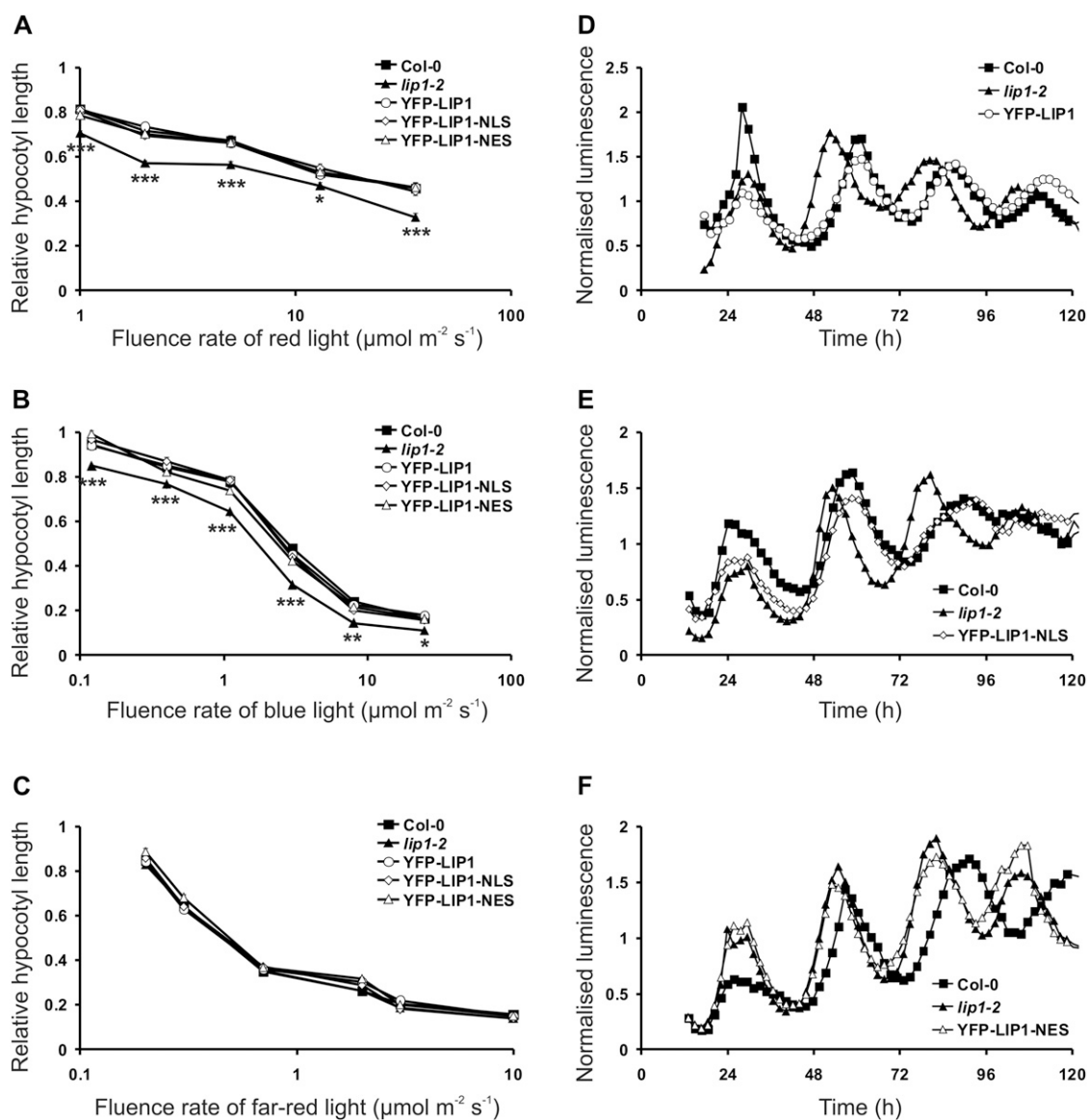
Figure 7. Complementation of photomorphogenic and circadian phenotypes of *lip1-2* by LIP1 fusion proteins. A to C, Fluence rate curves of hypocotyl elongation in cR (A), cB (B), or cFR (C). Col-0 (black squares), *lip1-2* (black triangles), and seedlings expressing YFP-LIP1 (white circles), YFP-LIP1-NLS (white diamonds), or YFP-LIP1-NES (white triangles) fusion proteins in the *lip1-2* background were grown in constant monochromatic light at the indicated fluence rates for 4 d, then hypocotyl length of the seedlings was measured. Values were normalized to the hypocotyl length of the corresponding dark-grown seedlings. The *x* axes show logarithmic scale ($n = 28$–32). Error bars represent SE. Irrespective of the light conditions, no significant differences were detected between the wild type and either of the transgenic lines (one-way ANOVA, Tukey's test). Hence, asterisks indicate significant differences between *lip1-2* and the wild type as determined by Student's *t* test: $*P < 0.05$, $**P < 0.01$, $***P < 0.001$. D to F, Col-0 (black squares), *lip1-2* mutants (black triangles), and *lip1-2* mutants expressing YFP-LIP1 (white circles; D), YFP-LIP1-NLS (white diamonds; E), or YFP-LIP1-NES (white triangles; F) fusion proteins were grown in 12:12 LD cycles for 7 d and transferred to cR at 3 μmol m^{-2} s^{-1} fluence rate. Rhythmic luminescence of the *CAB2:LUC* marker was measured, and values normalized to the mean were plotted. Three independent transgenic lines were measured for each construct with similar results. Representative graphs are shown.

ROS-linked small GTPases are localized mostly in the plasma membrane, which is in contrast with the nucleocytoplasmic localization of LIP1 (Supplemental Fig. S9) and the complementation of stress hypersensitivity by the nucleus-targeted LIP1 protein (Fig. 5).

Despite these differences, it is tempting to speculate that alterations in cell morphology and cell death in the epidermis could affect the "barrier" function of this cell layer in the *lip1* mutants, so that the excess of salt taken up cannot be compensated by the otherwise

intact salt signaling and response system. However, dark-grown *lip1* mutants without apparent cell morphology phenotypes were also hypersensitive to salt stress; therefore, we conclude that the salt sensitivity of *lip1* mutants is not caused by abnormally shaped (or missing) pavement cells.

The shortening of the circadian period by the *lip1* mutation is clearly detectable in etiolated plants (Kevei et al., 2007), where ploidy levels of *lip1* mutants do not differ from that of the wild type. On the other hand, the salt sensitivity, photomorphogenic, and ploidy phenotypes of *lip1* mutants could be detected under conditions where the mutants did not show circadian defects (i.e. high fluence rate of red or white light; Kevei et al., 2007). These facts strongly suggest that (1) the circadian function of LIP1 is independent from its other functions and (2) the altered function of the clock in the *lip1* mutants is not the cause of the stress, ploidy, or hypocotyl phenotype. This conclusion is further corroborated by the results of the complementation experiments. The circadian phenotype was complemented by YFP-LIP1 and YFP-LIP1-NLS but not by YFP-LIP1-NES, indicating that LIP1 must accumulate to a critical level in the nucleus in order to regulate the clock. The full complementation of the circadian phenotype also suggests that LIP1 does not affect clock-related cytosolic processes, although its role in mediating the nucleocytoplasmic partitioning of clock components cannot be excluded. Interestingly, all the other phenotypes were equally complemented by YFP-LIP1, YFP-LIP1-NLS, or YFP-LIP1-NES. It must be noted, however, that although the addition of NLS or NES motifs dramatically alters the subcellular localization of LIP1, by no means does it completely restrict the protein to the nucleus or the cytoplasm. Particularly, the NES motif does not prevent nuclear import but facilitates nuclear export, thereby reducing the average time spent by the tagged LIP1 protein in the nucleus. It follows that the very small amount of YFP-LIP1-NES present in the nucleus could be sufficient to mediate certain functions (e.g. controlling endoreplication). This amount is clearly insufficient for restoring circadian functions, demonstrating the great demand of the clock for nuclear LIP1. However, it would be premature to designate certain cellular compartments as locations of LIP1 protein fractions affecting salt stress, photomorphogenesis, or endoreplication.

In plants, LIP1 is the founder of a novel and, therefore, not well-characterized subclass of small GTPases, and it is the only small GTPase that has been functionally linked to the regulation of the circadian clock (Kevei et al., 2007). Interestingly, some members of the ROP and RAB subfamilies were shown to modulate responses similar to LIP1. For example, ROP GTPases (ROP2, -4, and -6) were reported to control the shape of pavement cells via the assembly and organization of cortical microfilament and microtubule networks (Fu et al., 2005, 2009). Arabidopsis RAB GTPASE6 is a RAB-type GTPase implicated in vesicular trafficking between endosomes and the plasma membrane, and similar to

LIP1, it is required for tolerance to high salinity (Ebine et al., 2011). More recently, it has been suggested that the activity of the ROP8 GTPase is regulated by phytochromes, which probably accounts for light-dependent control of root elongation by ROP8 (Shin et al., 2010). However, further studies are required to elucidate the molecular mechanisms by which the functions of these small GTPases are integrated at the cellular level.

Our results indicate that LIP1 facilitates germination under suboptimal conditions, entrains the circadian clock in plants germinating/elongating in the soil at limited light intensities, and controls the normal morphology of the emerged young seedlings; therefore, we suggest that LIP1 is an important modulator of seedling establishment. However, it is unlikely that all functions of LIP1 are limited to the seedling stage, since LIP1 is clearly expressed in most tissues of adult plants. The lack of cell shape and ploidy phenotypes in adult *lip1* mutant plants can be explained by the presence of developmentally regulated proteins functionally redundant to LIP1 or by the availability of different interacting partners at different developmental stages. The identification of conformation-specific interacting proteins, which regulate the activity of LIP1 or act as effectors downstream of LIP1, will be essential for delineating the molecular function of this small GTPase in diverse signaling cascades.

MATERIALS AND METHODS

Plant Materials and Growth Conditions

Arabidopsis (*Arabidopsis thaliana*) ecotypes C24 and Col-0 were used as wild-type plants. *lip1-1* and *lip1-2* alleles are in the C24 and Col-0 backgrounds, respectively (Kevei et al., 2007). The *phyA-211*, *phyB-9*, and *cry1-304 cry2-1* mutants (all in the Col-0 ecotype) have been described (Reed et al., 1993; Reed and Chory, 1994; Mockler et al., 1999). The *cry1-304 cry2-1* double mutant is referred to as *cry1 cry2* here. Surface-sterilized seeds were stratified at 4°C for 3 d and grown in 12:12 LD photocycles at 22°C for 7 d unless indicated otherwise. Seedlings for ploidy level measurements, cell morphology determinations, and *DEL1* qRT-PCR assays were grown on one-half-strength Murashige and Skoog medium supplemented with 1% (w/v) Suc. Plants for luminescence detection, salt tolerance tests, and the investigation of salt-induced gene expression were grown on Murashige and Skoog medium supplemented with 3% (w/v) Suc. For hypocotyl elongation tests, seedlings were sown on wet filter paper. Special growth conditions are described below or in the corresponding figure legends.

Gene Constructs and Transgenic Plants

Transgenic *lip1-1* plants expressing the YFP-LIP1 fusion protein under the control of the cauliflower mosaic virus 35S promoter, and the modified pPCV812 binary vectors containing the 35S promoter and DNA fragments coding for YFP and NLS or NES motifs, have been described (Kevei et al., 2007; Palágyi et al., 2010). To create 35S:YFP-LIP1-NLS/NES constructs, the LIP1 complementary DNA fragment was inserted in the modified pPCV812 vectors between the YFP and NLS/NES fragments. The constructs were transformed in *lip1-1* and *lip1-2* mutant plants expressing the *CAB2:LUC* marker (Clough and Bent, 1998). Transformants were selected on Murashige and Skoog medium supplemented with 15 μg mL^{-1} hygromycin. Ten to 15 independent transformants for each construct were self-fertilized, and individuals of the homozygous T3 progeny were used for experiments.

Scanning Electron Microscopy

Scanning electron microscopy was carried out using a Zeiss Supra 40VP (Carl Zeiss) equipped with a field emission gun as electron source, secondary electron detector for imaging, and combined with the Emitech K1250X (Quorum Emitech) transfer system. The biological samples were prepared with a cryogenic preparation method. Fresh tissue parts were mounted onto the probe holder using Tissue-Tec (O.C.T. Compound) as glue, and gold/palladium was used for sputter coating.

Differential Interference Contrast Microscopy and Calculation of Shape Factor

Seven-day-old seedlings were cleared overnight in a solution composed of 160 g of chloral hydrate (Sigma-Aldrich), 100 mL of water, and 50 mL of glycerol. After clearing, cotyledons were mounted with a coverslip, and pavement cells were visualized with a Leica DMRB microscope equipped with differential interference contrast microscopy optics. Images were captured on a Leica DFC 490 camera using the Leica Application Suite 2.5.0 software. Cell area and the perimeter of matured pavement cells were measured with ImageJ software, and shape factor was calculated as 4π area/perimeter^2. Statistical significance was assessed with Student's t test calculated with SigmaStat 3.5 software.

Confocal Laser-Scanning Microscopy

Cotyledons of 7-d-old seedlings were mounted on glass slides, and fluorescence was detected with the Leica TCS SP2 AOBS confocal laser-scanning microscopy system equipped with 40× and 63× lenses, an argon-krypton laser, and a 405-nm diode laser (Leica).

Ploidy Measurement with Flow Cytometry

Plant material was cut with a razor blade, stained with the CyStain UV precise P DNA staining kit (Partec), and then filtered though 50-μm mesh. The ploidy level of samples was measured with Ploidy Analyzer PA-1 (Partec) and analyzed with FloMax 2.52 software (Partec). Statistical significance was calculated with SigmaStat 3.5 software.

Physiological Assays

For luminescence detection, seedlings were grown in 12:12 LD cycles for 7 d and transferred to cR (SnapLite; Quantum Devices) at 5 μmol m^{-2} s^{-1} fluence rate. Luminescence was monitored for 4 d using the TopCount NXT luminometer (Perkin-Elmer) as described (Kevei et al., 2007). Counts were normalized to the average of counts collected during the entire measurement and were plotted as normalized luminescence.

For salt tolerance assays, seedlings were germinated in 12:12 LD cycles for 14 d on medium containing NaCl at different concentrations. To test the effect of high salinity on germination rate, seeds were sown on medium with or without 200 mM NaCl. The plates were transferred to 12:12 LD or to constant darkness. Germinated seeds with clearly visible radicles were counted daily for 5 d. To assess germination on subsequent days in darkness, separate plates were moved to light on each day and germinating seedlings were counted. For root length measurements, seedlings were grown in 12:12 LD cycles for 7 d on salt-free medium and transferred to medium supplemented with different concentrations of NaCl. The plates were set to vertical position, and the length of roots was measured 7 d after the transfer. Values were normalized to the length of roots of nontreated plants.

Hypocotyl lengths were measured essentially as described (Palágyi et al., 2010).

Analysis of Gene Expression

To determine *DEL1* mRNA levels, plants were grown in cR (40 μmol m^{-2} s^{-1}) or in darkness for 7 d before samples were harvested. To measure *RD29A*, *RD29B*, *RAB18*, and *SOS2* mRNA levels, plants were grown in 12:12 LD cycles for 7 d and transferred to medium with or without 200 mM NaCl, and samples were harvested 1, 3, 6, 9, and 12 h after the transfer. Isolation of total RNA, complementary DNA synthesis, and qRT-PCR were carried out as described (Palágyi et al., 2010). Specific mRNA levels were normalized to *TUBULIN2/3* mRNA levels in each sample. Sequences of primers used for qRT-PCR assays are shown in Supplemental Table S1. Averages of results from three independent experiments are shown; error bars represent SE values. For procedures of protein extraction and western analysis see Supplemental Materials and Methods S1.

Supplemental Data

The following materials are available in the online version of this article.

Supplemental Figure S1. Noncontinuous cell layer in the epidermis of cotyledons in *lip1-2* mutants.

Supplemental Figure S2. Pavement cell morphology in etiolated plants.

Supplemental Figure S3. Statistical analysis of ploidy measurements in darkness and cR.

Supplemental Figure S4. Statistical analysis of ploidy measurements in darkness and cB.

Supplemental Figure S5. Statistical analysis of hypocotyl measurements in cR, cB, and cFR.

Supplemental Figure S6. Absolute hypocotyl length data for Figure 5, A to C.

Supplemental Figure S7. *lip1* mutant plants are hypersensitive to salt.

Supplemental Figure S8. Effect of LIP1 on salt stress-induced gene expression.

Supplemental Figure S9. Manipulation of subcellular localization of YFP-LIP1 fusion proteins.

Supplemental Figure S10. Complementation of the cell shape phenotype of *lip1-1* mutants.

Supplemental Table S1. Sequences of primers used for qRT-PCR assays.

Supplemental Materials and Methods S1.

LITERATURE CITED

Berckmans B, Lammens T, Van Den Daele H, Magyar Z, Bögre L, De Veylder L (2011) Light-dependent regulation of DEL1 is determined by the antagonistic action of E2Fb and E2Fc. Plant Physiol **157:** 1440–1451

Chaves I, Pokorny R, Byrdin M, Hoang N, Ritz T, Brettel K, Essen LO, van der Horst GT, Batschauer A, Ahmad M (2011) The cryptochromes: blue light photoreceptors in plants and animals. Annu Rev Plant Biol **62:** 335–364

Clough SJ, Bent AF (1998) Floral dip: a simplified method for Agrobacterium-mediated transformation of Arabidopsis thaliana. Plant J **16:** 735–743

Covington MF, Maloof JN, Straume M, Kay SA, Harmer SL (2008) Global transcriptome analysis reveals circadian regulation of key pathways in plant growth and development. Genome Biol **9:** R130

De Veylder L, Larkin JC, Schnittger A (2011) Molecular control and function of endoreplication in development and physiology. Trends Plant Sci **16:** 624–634

Devlin PF, Kay SA (2000) Cryptochromes are required for phytochrome signaling to the circadian clock but not for rhythmicity. Plant Cell **12:** 2499–2510

Dodd AN, Salathia N, Hall A, Kévei E, Tóth R, Nagy F, Hibberd JM, Millar AJ, Webb AA (2005) Plant circadian clocks increase photosynthesis, growth, survival, and competitive advantage. Science **309:** 630–633

Dong MA, Farré EM, Thomashow MF (2011) Circadian clock-associated 1 and late elongated hypocotyl regulate expression of the C-repeat binding factor (CBF) pathway in Arabidopsis. Proc Natl Acad Sci USA **108:** 7241–7246

Ebine K, Fujimoto M, Okatani Y, Nishiyama T, Goh T, Ito E, Dainobu T, Nishitani A, Uemura T, Sato MH, et al (2011) A membrane trafficking pathway regulated by the plant-specific RAB GTPase ARA6. Nat Cell Biol **13:** 853–859

Finkel T (2006) Intracellular redox regulation by the family of small GTPases. Antioxid Redox Signal **8:** 1857–1863

Franklin KA, Quail PH (2010) Phytochrome functions in Arabidopsis development. J Exp Bot **61:** 11–24

Fu Y, Gu Y, Zheng Z, Wasteneys G, Yang Z (2005) Arabidopsis interdigitating cell growth requires two antagonistic pathways with opposing action on cell morphogenesis. Cell **120:** 687–700

Fu Y, Xu T, Zhu L, Wen M, Yang Z (2009) A ROP GTPase signaling pathway controls cortical microtubule ordering and cell expansion in Arabidopsis. Curr Biol **19:** 1827–1832

Fukushima A, Kusano M, Nakamichi N, Kobayashi M, Hayashi N, Sakakibara H, Mizuno T, Saito K (2009) Impact of clock-associated Arabidopsis pseudo-response regulators in metabolic coordination. Proc Natl Acad Sci USA **106:** 7251–7256

Gendreau E, Höfte H, Grandjean O, Brown S, Traas J (1998) Phytochrome controls the number of endoreduplication cycles in the Arabidopsis thaliana hypocotyl. Plant J **13:** 221–230

Guimil S, Dunand C (2007) Cell growth and differentiation in Arabidopsis epidermal cells. J Exp Bot **58:** 3829–3840

Huang W, Pérez-García P, Pokhilko A, Millar AJ, Antoshechkin I, Riechmann JL, Mas P (2012) Mapping the core of the Arabidopsis circadian clock defines the network structure of the oscillator. Science **336:** 75–79

Kant P, Gordon M, Kant S, Zolla G, Davydov O, Heimer YM, Chalifa-Caspi V, Shaked R, Barak S (2008) Functional-genomics-based identification of genes that regulate Arabidopsis responses to multiple abiotic stresses. Plant Cell Environ **31:** 697–714

Kevei E, Gyula P, Fehér B, Tóth R, Viczián A, Kircher S, Rea D, Dorjgotov D, Schäfer E, Millar AJ, et al (2007) Arabidopsis thaliana circadian clock is regulated by the small GTPase LIP1. Curr Biol **17:** 1456–1464

Kevei E, Gyula P, Hall A, Kozma-Bognár L, Kim WY, Eriksson ME, Tóth R, Hanano S, Fehér B, Southern MM, et al (2006) Forward genetic analysis of the circadian clock separates the multiple functions of ZEITLUPE. Plant Physiol **140:** 933–945

Lammens T, Boudolf V, Kheibarshekan L, Zalmas LP, Gaamouche T, Maes S, Vanstraelen M, Kondorosi E, La Thangue NB, Govaerts W, et al (2008) Atypical E2F activity restrains APC/CCCS52A2 function obligatory for endocycle onset. Proc Natl Acad Sci USA **105:** 14721–14726

Legnaioli T, Cuevas J, Mas P (2009) TOC1 functions as a molecular switch connecting the circadian clock with plant responses to drought. EMBO J **28:** 3745–3757

Más P (2008) Circadian clock function in Arabidopsis thaliana: time beyond transcription. Trends Cell Biol **18:** 273–281

Mockler TC, Guo H, Yang H, Duong H, Lin C (1999) Antagonistic actions of Arabidopsis cryptochromes and phytochrome B in the regulation of floral induction. Development **126:** 2073–2082

Nakamichi N, Kusano M, Fukushima A, Kita M, Ito S, Yamashino T, Saito K, Sakakibara H, Mizuno T (2009) Transcript profiling of an Arabidopsis PSEUDO RESPONSE REGULATOR arrhythmic triple mutant reveals a role for the circadian clock in cold stress response. Plant Cell Physiol **50:** 447–462

Ono E, Wong HL, Kawasaki T, Hasegawa M, Kodama O, Shimamoto K (2001) Essential role of the small GTPase Rac in disease resistance of rice. Proc Natl Acad Sci USA **98:** 759–764

Palágyi A, Terecskei K, Adám E, Kevei E, Kircher S, Mérai Z, Schäfer E, Nagy F, Kozma-Bognár L (2010) Functional analysis of amino-terminal domains of the photoreceptor phytochrome B. Plant Physiol **153:** 1834–1845

Park J, Gu Y, Lee Y, Yang Z, Lee Y (2004) Phosphatidic acid induces leaf cell death in Arabidopsis by activating the Rho-related small G protein GTPase-mediated pathway of reactive oxygen species generation. Plant Physiol **134:** 129–136

Pruneda-Paz JL, Kay SA (2010) An expanding universe of circadian networks in higher plants. Trends Plant Sci **15:** 259–265

Reed JW, Chory J (1994) Mutational analyses of light-controlled seedling development in Arabidopsis. Semin Cell Biol **5:** 327–334

Reed JW, Nagpal P, Poole DS, Furuya M, Chory J (1993) Mutations in the gene for the red/far-red light receptor phytochrome B alter cell elongation and physiological responses throughout *Arabidopsis* development. Plant Cell **5:** 147–157

Rizzini L, Favory JJ, Cloix C, Faggionato D, O'Hara A, Kaiserli E, Baumeister R, Schäfer E, Nagy F, Jenkins GI, et al (2011) Perception of UV-B by the Arabidopsis UVR8 protein. Science **332:** 103–106

Sanchez A, Shin J, Davis SJ (2011) Abiotic stress and the plant circadian clock. Plant Signal Behav **6:** 223–231

Shin DH, Cho MH, Kim TL, Yoo J, Kim JI, Han YJ, Song PS, Jeon JS, Bhoo SH, Hahn TR (2010) A small GTPase activator protein interacts with cytoplasmic phytochromes in regulating root development. J Biol Chem **285:** 32151–32159

Verkest A, Manes CL, Vercruysse S, Maes S, Van Der Schueren E, Beeckman T, Genschik P, Kuiper M, Inzé D, De Veylder L (2005) The cyclin-dependent kinase inhibitor KRP2 controls the onset of the endoreduplication cycle during *Arabidopsis* leaf development through inhibition of mitotic CDKA;1 kinase complexes. Plant Cell **17:** 1723–1736

Wang L, Fujiwara S, Somers DE (2010) PRR5 regulates phosphorylation, nuclear import and subnuclear localization of TOC1 in the Arabidopsis circadian clock. EMBO J **29:** 1903–1915

Wong HL, Pinontoan R, Hayashi K, Tabata R, Yaeno T, Hasegawa K, Kojima C, Yoshioka H, Iba K, Kawasaki T, et al (2007) Regulation of rice NADPH oxidase by binding of Rac GTPase to its N-terminal extension. Plant Cell **19:** 4022–4034

Yamaguchi-Shinozaki K, Shinozaki K (2006) Transcriptional regulatory networks in cellular responses and tolerance to dehydration and cold stresses. Annu Rev Plant Biol **57:** 781–803